

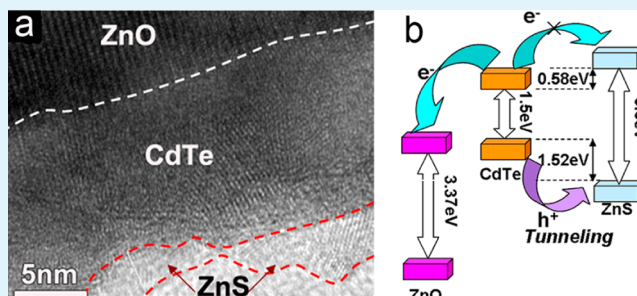
# Dual Roles of ZnS Thin Layers in Significant Photocurrent Enhancement of ZnO/CdTe Nanocable Arrays Photoanode

Xina Wang, Rong Liu, Tian Wang, Baoyuan Wang, Yang Xu, and Hao Wang\*

Hubei Collaborative Innovation Center for Advanced Organic Chemical Materials, Faculty of Physics and Electronic Technology, Hubei University, Wuhan 430062, PR China

**ABSTRACT:** The effect of a ZnS thin layer on the photoelectrochemical property of ZnO/CdTe nanocable arrays-on-indium tin oxide was systematically studied by the successive ion layer absorption and reaction (SILAR) of ZnS. The thickness of CdTe on bare ZnO/CdTe nanocable arrays was optimized to approximately 10 nm to achieve a saturated photocurrent density of 6.5 mA/cm<sup>2</sup>. Significant photocurrent enhancement was achieved by gradually increasing the ZnS SILAR cycle number from 0 to 10. A “type I” band alignment with conduction and valence band offsets of 0.58 and 1.52 eV, respectively, was deduced for the CdTe/ZnS interface. The detailed microstructure of the CdTe/ZnS interface and the relationship between the photocurrent and the ZnS thickness indicated that ZnS not only serves as a barrier layer that prevents electron injection from CdTe to the electrolyte but also provides an effective tunneling channel for hole transfers to the electrolyte. A ZnO/CdTe/ZnS nanocable photoanode yielded a saturated photocurrent density of 13.8 mA/cm<sup>2</sup> when the thickness of ZnS was controlled to approximately 2 nm.

**KEYWORDS:** ZnO/CdTe, ZnS, passivation, photoelectrochemical property



## 1. INTRODUCTION

Narrow band gap semiconductor quantum dots (QDs), such as PbS,<sup>1,2</sup> PbSe,<sup>3</sup> InP,<sup>4</sup> InAs,<sup>5</sup> CdS,<sup>6,7</sup> CdSe,<sup>8–10</sup> and CdTe,<sup>11,12</sup> have recently been adopted as effective sensitizers in QD sensitized solar cells (QDSSCs) because of their unique size and shape-dependent absorption properties.<sup>13</sup> Improved photovoltaic properties may be established when the QDs are loaded onto one-dimensional (1D) ZnO nanorod and/or TiO<sub>2</sub> nanotube arrays on an electric conductive substrate, the configuration of which is greatly beneficial to both carrier injection at the nanoarray/QD interface and carrier transport in the 1D electrode.<sup>14–24</sup> However, the cell conversion efficiency of such arrays is restricted because of the low loading density of QDs on the 1D electrodes and nonradiative recombination processes that occur on the 1D oxide/electrolyte, QD/electrolyte, and QD/QD interfaces.<sup>25</sup> To address these issues, core–sheath nanocable structures, such as ZnO/Zn<sub>x</sub>Cd<sub>1-x</sub>Se,<sup>26</sup> ZnO/CdTe,<sup>27</sup> ZnO/CdSe,<sup>28</sup> ZnO/CdSSe,<sup>29</sup> ZnO/CdS,<sup>30</sup> ZnO/CdSe/CdTe,<sup>31</sup> and TiO<sub>2</sub>/In<sub>2</sub>S<sub>3</sub>,<sup>32</sup> have successfully been constructed as photoanodes of solar cells. Improved performance has been established over traditional QDSSCs using narrow-gap semiconductors as shells and single-crystalline ZnO or TiO<sub>2</sub> 1D arrays as cores. The improvements observed are attributed to the high loading density of the continuous sensitizer layer, the low recombination interface of the oxide/electrolyte, and fast carrier separation along the radial direction of the nanocables. CdTe and Zn<sub>x</sub>Cd<sub>1-x</sub>Se-sensitized nanocable arrays present higher short-circuit currents than CdS and CdSe arrays because of the narrower band gap of the former, which

greatly expands the absorption spectrum.<sup>26,27</sup> Unfortunately, most nanoshells of these nanocable electrodes are composed of randomly grown nanocrystals on the surface of ZnO nanowires that may introduce nonradiative recombination at the grain boundaries and around surface defects.<sup>26,33</sup> Therefore, thickness control and surface passivation of sensitizer nanoshells are important issues for the improvement of the photovoltaic performance of nanocable arrays.

As a wide band gap semiconductor, ZnS has been extensively deposited on QDs on the surface of QDSSC photoanodes to suppress electron leakage from QDs to the electrolyte.<sup>34–39</sup> In addition, the conduction band minimum of ZnS always lies above that of CdTe,<sup>40</sup> making ZnS a potential passivation layer for ZnO/CdTe nanocable photoanodes. However, studies on the surface passivation of ZnO/CdTe nanocable arrays have yet to be reported. While ZnS is known to serve as a barrier layer for electron injections from the absorbing layer to the electrolyte, hole transfers to the electrolyte may be impeded when considering the lower valence band level of ZnS compared with that of many other semiconductor absorbers. Therefore, a detailed description of the passivation mechanism in ZnS during hole transfer must be elucidated.

In this study, the effect of CdTe thickness on the photoelectrochemical (PEC) property of ZnO/CdTe nanocable arrays-on-indium tin oxide (ITO) was systematically

Received: January 28, 2013

Accepted: March 21, 2013

Published: March 21, 2013

investigated. Based on the optimized thickness, ZnO/CdTe nanocable arrays were passivated by ZnS of various thicknesses. A saturated photocurrent as high as 13.8 mA/cm<sup>2</sup> was obtained after decoration of the nanocables with ZnS with thicknesses between 2 and 5 nm. A detailed passivation mechanism was also proposed based on the energy level alignment and microstructure of the ZnO/CdTe/ZnS nanocable arrays.

## 2. EXPERIMENTAL SECTION

**2.1. Preparation Process of ZnO/CdTe/ZnS Nanocable Photoanodes.** ZnO nanorod arrays were grown on an ITO substrate by the hydrothermal method,<sup>41–43</sup> during which 0.025 M zinc acetate and 0.025 M hexamethylene tetraamine were held at 92 °C for 5 h in a Teflon-sealed autoclave. CdTe was electrodeposited on the ZnO arrays to form a core–sheath nanocable structure using an electrochemical workstation (CHI instrument, model 660D) with a three-electrode system at room temperature. ZnO nanorod arrays-on-ITO, Pt foil, and saturated calomel electrode served as the working, counter, and reference electrodes, respectively. The electrolyte was composed of 0.05 M potassium tellurite (K<sub>2</sub>TeO<sub>3</sub>), 0.5 mM nitrilotriacetic acid trisodium (C<sub>6</sub>H<sub>6</sub>NO<sub>6</sub>K<sub>3</sub>, NTA), and 0.2 M cadmium acetate. The thickness of CdTe on ZnO was adjusted by changing the charge density passing through the electrode from 0.6 to 1.1 C/cm<sup>2</sup>. After electrodeposition, the samples were annealed at 350 °C for 1 h under a nitrogen atmosphere. A ZnS overlayer was synthesized on the ZnO/CdTe nanocable arrays-on-ITO through a traditional successive ion layer absorption and reaction (SILAR) method<sup>44</sup> by immersion in 0.02 M acetate zinc in ethanol and 0.02 M Na<sub>2</sub>S for 2 to 15 cycles. After each cycle, the sample was rinsed with distilled water and air dried. The final products were annealed at 300 °C for 1 h.

**2.2. Characterization.** The morphology, crystallinity, and optical property of the samples were characterized by scanning electron microscopy (FE-SEM, JEOL, JSM-6700F), X-ray diffraction (XRD, D8), and UV–vis–IR absorption spectroscopy (UV360 spectrometer), respectively. The microstructure and elemental compositions of the sample were studied using a scanning transmission electron microscope (STEM, TEM, Tecnai model 20 FEI) equipped with an energy dispersive X-ray spectrometer (EDX). The PEC property of the ZnO/CdTe/ZnS nanocable array electrodes was determined using the same electrochemical workstation used for electrodeposition under illumination of AM 1.5G simulated sunlight. In this experiment, a saturated Ag/AgCl electrode and Pt foil were used as the reference and counter electrodes, respectively. The electrolyte used was composed of a mixed solution of methanol and water (v/v = 7:3) with 0.1 M KCl, 0.1 M Na<sub>2</sub>S, and 0.3 M sulfur.

## 3. RESULTS AND DISCUSSION

**3.1. Microstructure and Absorption Property of ZnO/CdTe/ZnS Nanocable Arrays.** Figure 1a–d shows SEM images, which show the morphology evolution from ZnO nanowires to ZnO/CdTe then to ZnO/CdTe/ZnS nanocable

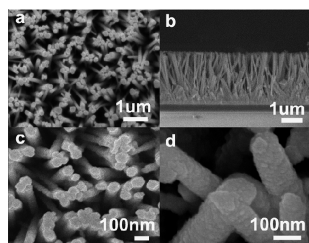


**Figure 1.** Top-view (a) and cross-sectional (b) SEM images of ZnO nanorod arrays on ITO substrate. Panels c and d show the top-view SEM images of ZnO/CdTe core–shell nanocable arrays before and after ZnS decoration, respectively.

arrays. Figure 1a and b shows that the ZnO nanowires grow vertically on the ITO substrate with an average diameter and length of ~120 nm and ~2.8 μm, respectively. After CdTe electrodeposition with a total charge density of 0.6 C, the ZnO nanowires were completely covered by CdTe nanocrystals, forming a core–shell ZnO/CdTe nanocable structure. The shell thickness was estimated to be ~10 nm by comparing the change in diameter of ZnO before and after CdTe deposition (Figure 1a and c). Figure 1d shows an SEM image of the ZnO/CdTe nanocable arrays after ZnS decoration via 10 SILAR cycles. ZnS nanocrystals with sizes less than 15 nm can be clearly observed on the surface of the CdTe nanoshells. The thickness of ZnS on CdTe may be tuned by varying the number of SILAR cycles from 2 to 15.

Figure 2 shows the XRD spectra of pure ZnO nanowire arrays (plot a) and ZnO/CdTe nanocable arrays before (plot

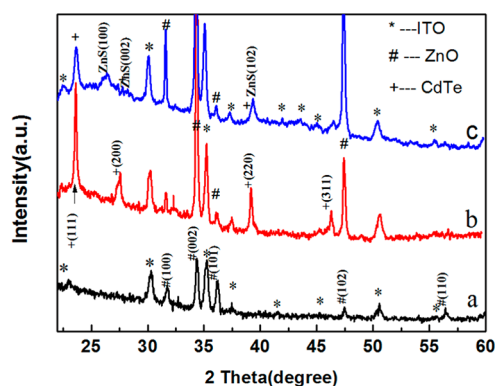


**Figure 2.** XRD patterns of ZnO nanorod arrays on ITO (a), ZnO/CdTe nanocable arrays before (b) and after (c) decoration of ZnS.

b) and after ZnS decoration (plot c). Diffraction peaks of the pure ZnO nanowires at 34.3°, 31.7°, and 47.4° can be indexed to the (002), (100), and (102) planes of wurtzite ZnO (JCPDS No. 89-1397), respectively. After electrodeposition of CdTe, four additional diffraction peaks appeared at 23.7°, 27.5°, 39.2°, and 46.4° corresponding to the (111), (200), (220), and (311) planes of cubic CdTe (JCPDS No. 65-880), respectively. The full width at half-maximum of the diffraction peak of CdTe (200) is 0.0028 in radian, suggesting that the size of the CdTe nanoparticles is about 52 nm, as estimated from the Scherrer formula ( $D = 0.89\lambda/B \cos \theta$ ), where  $\lambda$  and  $B$  are 1.54 Å and 0.0028, respectively. After 10 ZnS SILAR cycles, three diffraction peaks can be found at 26.9°, 28.6°, and 39.6°; these peaks can be indexed to the (100), (002), and (102) planes of wurtzite ZnS (JCPDS No. 89-2942), respectively. The weak and broad diffraction peaks indicate that the size of the ZnS nanocrystals is very small, corresponding to the physical characteristics of materials obtained from the SILAR method.

The evolution of optical absorption properties from ZnO nanowires to ZnO/CdTe/ZnS nanocables is shown in Figure 3. An absorption edge shift from 378 to 820 nm can be clearly seen after CdTe deposition, corresponding well with the band gap of CdTe (1.5 eV).<sup>45</sup> A blue shift to ~750 nm occurs after ZnS decoration of ZnO/CdTe, indicating that the absorption ability is slightly weakened by ZnS nanocrystals on the exterior of the wires with wider band gaps. This phenomenon is quite similar with the blue shift in photoluminescence and absorption of CuInS<sub>2</sub>/ZnS core/shell quantum dots, for which three possible reasons including surface reconstruction, cation

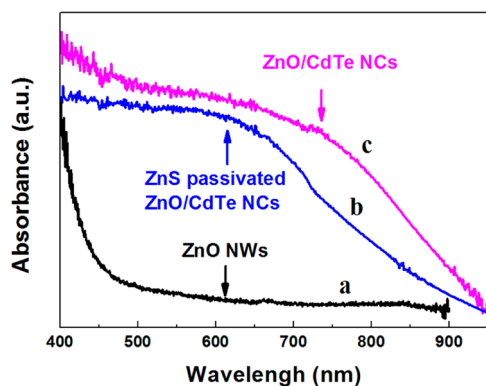


**Figure 3.** Absorption spectra of ZnO nanorod arrays and ZnO/CdTe nanocable arrays before and after decoration of ZnS.

exchange at the core/shell interface and interdiffusion of Zn atoms were proposed.<sup>46–48</sup> For our ZnO/CdTe/ZnS nanocables, the blue shift maybe caused by the reaction of Cd cations with S anions and/or interdiffusion of Zn or Cd atoms both occurred at the CdTe/ZnS interface during the SILAR and annealing process.

TEM-related measurements were performed to further study the evolution of microstructures before and after decoration of the ZnO/CdTe nanocables with ZnS. Figure 4a shows a low-magnification TEM image of a single ZnO/CdTe nanocable. A CdTe shell with a thickness of  $\sim 10$  nm can be clearly found on the surface of the ZnO core, which has a diameter of  $\sim 120$  nm. The high-resolution transmission electron microscopy (HRTEM) image of the nanocable in Figure 4b suggests that

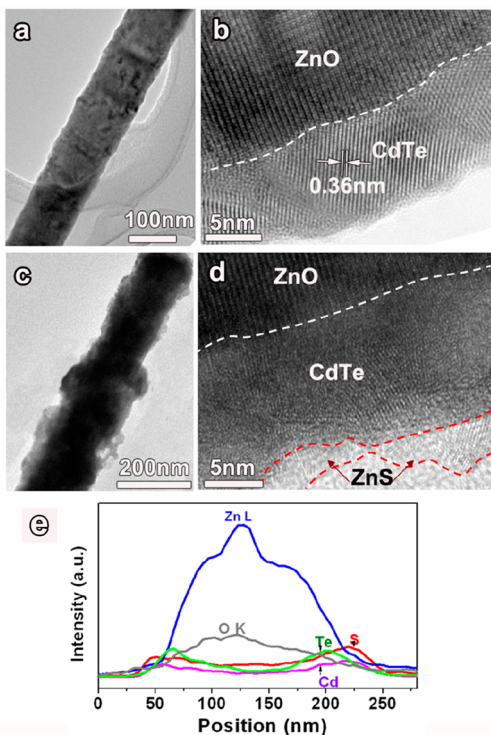


**Figure 4.** Low- and high-magnification TEM images of a single ZnO/CdTe (a and b) and a ZnO/CdTe/ZnS nanocable (c and d), respectively. Panel f gives the spectra of EDX line scans along the radial direction of the ZnO/CdTe/ZnS nanocable as shown in panels c and d.

ZnO is covered by a uniform CdTe layer of zinc-blende structure. Figure 4c and d shows low- and high-magnification TEM images of a single ZnO/CdTe/ZnS nanocable obtained after 10 SILAR cycles of ZnS. In these images, ZnS nanocrystals formed nonuniformly on the surface of CdTe. The sizes of the ZnS nanocrystals ranged from 2 to 5 nm. Compared with the dense CdTe layer, the distribution of ZnS nanocrystals was very sparse, resulting in a less continuous ZnS layer with nonhomogenous thickness. The configuration of the ZnO/CdTe/ZnS nanocable was further confirmed by EDX line scans along its radial direction. As shown by Figure 4e, S and Zn elements were first detected during the scanning, and the signal of Cd and Te were found in the shell region prior to the appearance of Zn and O elements in the core.

**3.2. Photoelectrochemical (PEC) Property of ZnO/CdTe Nanocable Arrays Decorated by ZnS Thin Layer.** The influence of thickness of the CdTe shell on the PEC properties of the ZnO/CdTe nanocable arrays was systematically studied. Figure 5 shows the photocurrent density versus

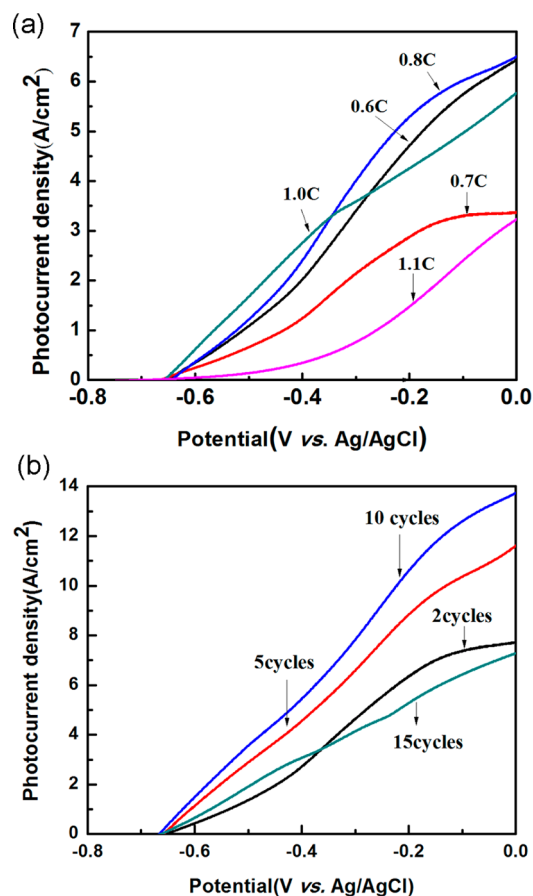


**Figure 5.** (a) Current density versus potential curves of bare ZnO/CdTe nanocable arrays with various electrodeposition charge density of CdTe and (b) ZnO/CdTe nanocable arrays decorated by ZnS with SILAR cycles ranging from 2 to 15. All of the above photoanodes were measured under the illumination of AM1.5G light.

potential ( $J$ - $V$ ) curves of ZnO/CdTe nanocable arrays under irradiation of AM 1.5 G simulated sunlight. When the electric quantity of CdTe during the deposition was 0.6 C, the photocurrent at 0 bias voltage was  $6.4 \text{ mA/cm}^2$ . The photocurrent slightly increased to  $6.5 \text{ mA/cm}^2$  as the electric quantity increased to 0.8 C. Further increases in electric

quantity to 1.1 C only led to the deterioration of the PEC property of the ZnO/CdTe photoanode. Since the CdTe shell thickness is directly related to the electric quantity during electrochemical deposition, the results suggest that the maximum photocurrent of the ZnO/CdTe nanocables could be achieved when the thickness of the CdTe shell is maintained at about 10 nm. A thinner shell may cause lower light absorption, which decreases the photocurrent, while a thicker shell may introduce more grain boundaries that can deteriorate carrier transfer along the radial direction of the nanocable.

On the basis of the optimum thickness of the CdTe layer, the effect of the ZnS overcast layer on the ZnO/CdTe nanocable arrays was investigated. Figure 5b shows the  $J$ - $V$  curves of ZnO/CdTe nanocables decorated by ZnS via 2–15 SILAR cycles. The photocurrent density of the photoanode increased to 7.7 mA/cm<sup>2</sup> at 0 bias voltage, when the ZnO/CdTe nanocables were coated by 2 SILAR cycles. The density linearly increased to 11.6 mA/cm<sup>2</sup> after 5 SILAR cycles and reached a maximum value of 13.8 mA/cm<sup>2</sup> at 0 bias voltage after 10 SILAR cycles, nearly a one-time enhancement in the photocurrent compared with bare ZnO/CdTe. Further ZnS deposition led to evident decreases in the photocurrent. These findings, combined with the HRTEM results, indicate that the maximal enhancement in photocurrent of the ZnO/CdTe photoanode occurs when the thickness of the ZnS passivation layer is maintained between 2 and 5 nm.

**3.3. Photocurrent Enhancement Mechanism for the ZnO/CdTe/ZnS Photoanodes.** To reveal the photocurrent enhancement mechanism of ZnS passivation, the band alignment of ZnO/CdTe/ZnS photoanode was further deduced by the flattened conduction band offset ( $\Delta E'_C$ ) after contact between CdTe and ZnS. Wei and Wang et al. reported that the  $\Delta E'_C$  can be calculated by  $\Delta E'_C = \Delta E_C - \Delta E_f$  if the difference in Fermi level ( $E_f$ ) and conduction band minimum ( $E_{CBM}$ ) is negligible.<sup>31,49</sup> In this study,  $\Delta E_C$  is defined as the unstrained conduction band offset between bulk CdTe and ZnS, the estimated value of which is 0.9 eV (Figure 7).<sup>40</sup>  $\Delta E_f$  is the total  $E_f$  shift in CdTe and ZnS after contact. Since the  $E_f$  values of the semiconductor and electrolyte become identical once electrostatic equilibrium is achieved, the  $E_f$  shift can be qualitatively evaluated by open circuit potentials deduced from dark current versus potential curves. From Figure 6, the equilibrium  $E_f$  of ZnO/CdTe, ZnO/ZnS, and ZnO/CdTe/ZnS nanocable anodes versus Ag/AgCl can be evaluated as  $-0.78$ ,

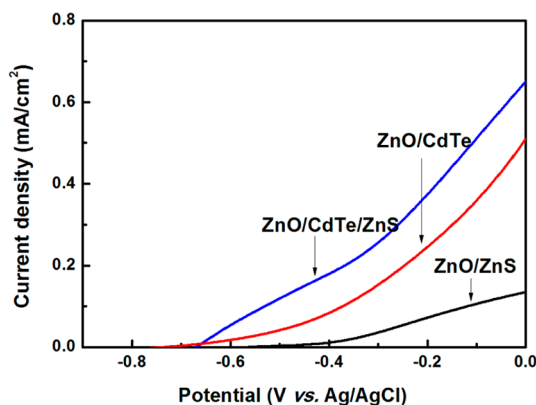


**Figure 6.** Current density versus potential curves of bare ZnO/CdTe, ZnO/ZnS, and ZnO/CdTe/ZnS nanocable arrays on ITO in dark conditions. The number of ZnO SILAR cycles is 10.

$-0.46$ , and  $-0.66$  eV, respectively. Figure 7 shows that an upward  $E_f$  shift of 0.12 eV and a downward  $E_f$  shift of 0.20 eV

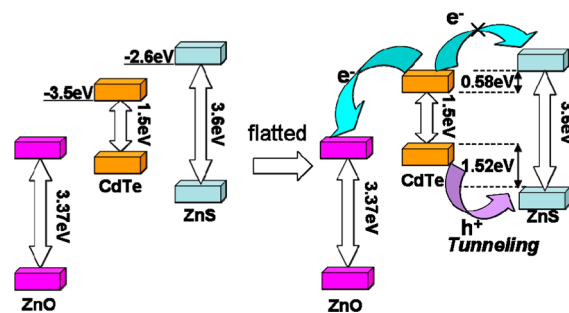


**Figure 7.** (a) Relative energy levels of bulk ZnO, CdTe, and ZnS<sup>40</sup> and (b) energy level alignment of the CdTe/ZnS interface for ZnO/CdTe/ZnS nanocable arrays.

occur in CdTe and ZnS, respectively, resulting in a total  $E_f$  shift ( $\Delta E_f$ ) of 0.32 eV and  $\Delta E'_C$  of 0.58 eV. This result suggests that an energy barrier of 0.58 eV is formed during the back transfer of photoexcited electrons from CdTe to the electrolyte via the ZnS layer, greatly reducing the recombination of electrons with the electrolyte.

The strained valence band offset ( $\Delta E'_V$ ) at the CdTe/ZnS interface can be evaluated as 1.52 eV using the formula  $\Delta E'_V = \Delta E_g - \Delta E'_C$ ,<sup>49</sup> where the difference in the bandgap of CdTe and ZnS ( $\Delta E_g$ ) is 2.1 eV. Combined with the positive value of  $\Delta E'_C$ , a “type I” band alignment occurs at the CdTe/ZnS interface of the nanocable photoanode. The higher  $E_{VBM}$  of CdTe compared with that of ZnS means that a potential barrier is formed for hole transport from CdTe to the electrolyte, contradicting the observed photocurrent enhancement by ZnS passivation. However, Hodes<sup>24</sup> suggested that even if the valence band edge of ZnS is below that of CdTe, hole transfer may still be possible if the ZnS layer is adequately thin such that hole tunneling or hole transfer through surface states in the ZnS layer is allowed. The ZnS layer over CdTe in the ZnO/CdTe/ZnS nanocable is discontinuous (Figure 4), with sizes ranging from 2 to 5 nm, and smaller ZnS nanocrystals may provide effective pathways for hole tunneling to the electrolyte. Such a deduction is further supported by the evolution of photocurrents in ZnO/CdTe/ZnS nanocable arrays with various ZnS thicknesses. The linear increase in photocurrent with increasing ZnS SILAR cycle numbers from 0 to 10 suggests that a thicker ZnS layer plays an important role in preventing electron injection from CdTe to the electrolyte. When the number of SILAR cycles is 15, the ZnS shell becomes too thick to allow hole tunneling to the electrolyte.

#### 4. SUMMARY

In conclusion, the effect of CdTe and ZnS thickness on the PEC property of ZnO/CdTe/ZnS nanocable arrays-on-ITO photoanodes was systematically studied. A maximum saturation current of 6.5 mA/cm<sup>2</sup> was obtained from a ZnO/CdTe nanocables photoanode with a CdTe shell thickness of  $\sim 10$  nm and a current density of 13.8 mA/cm<sup>2</sup> was observed after decoration of the nanocables by ZnS with an optimum thickness between 2 and 5 nm. A “type I” band alignment at the CdTe/ZnS interface was deduced for the ZnO/CdTe/ZnS nanocable photoanode; this alignment forms a potential barrier for electron injection to the electrolyte and ensures hole

transfer to the electrolyte via hole tunneling even when the thickness of ZnS is 2 nm.

## AUTHOR INFORMATION

### Corresponding Author

\*Fax: +86 27 88663390. E-mail: nanoguy@126.com.

### Notes

The authors declare no competing financial interest.

## ACKNOWLEDGMENTS

This work is supported in part by the National Nature Science Foundation of China (Nos. 51072049, 51102086), Research Fund for the Doctoral Program of Higher Education of China (RFD, No. 20104208120004), NSF and ED of Hubei Province (Nos. 2009CDA035, Z20091001, 2010BFA016, and Q20101006), and Wuhan Youth Chenguang Program of Science and Technology under Grant No. 2013070104010014. The authors thank Dr. H. J. Zhu for TEM characterization.

## REFERENCES

- (1) Plass, R.; Serge, P.; Kruger, J.; Grätzel, M.; Bach, U. *J. Phys. Chem. B* **2002**, *106*, 7578–7580.
- (2) Hoyer, P.; Könenkamp, R. *Appl. Phys. Lett.* **1995**, *66*, 349–351.
- (3) Schaller, R. D.; Klimov, V. I. *Phys. Rev. Lett.* **2004**, *92*, 186601.
- (4) Zaban, A.; Micić, O. I.; Gregg, B. A.; Nozik, A. J. *Langmuir* **1998**, *14*, 3153–3156.
- (5) Yu, P. R.; Zhu, K.; Norman, A. G.; Ferrere, S.; Frank, A. J.; Nozik, A. J. *J. Phys. Chem. B* **2006**, *110*, 25451–25454.
- (6) Chang, C. H.; Lee, Y. L. *Appl. Phys. Lett.* **2007**, *91*, 053503.
- (7) Robel, I.; Subramanian, V.; Kuno, M.; Kamat, P. V. *J. Am. Chem. Soc.* **2006**, *128*, 2385–2393.
- (8) Shen, Q.; Kobayashi, J. *J. Appl. Phys.* **2008**, *103*, 084304.
- (9) Niitsoo, O.; Sarkar, S. K.; Pejoux, C.; Ruhle, S.; Cahen, D. *J. Photochem. Photobiol. A* **2006**, *181*, 306–313.
- (10) Lee, Y.-H.; Huang, B.-M.; Chien, H.-T. *Chem. Mater.* **2008**, *20*, 6903–6905.
- (11) Cao, X.; Chen, P.; Guo, Y. *J. Phys. Chem. C* **2008**, *112*, 20560–20566.
- (12) Seabold, J. A.; Shankar, K.; Wilke, R. H. T. *Chem. Mater.* **2008**, *20*, 5266–5273.
- (13) Oregan, B.; Grätzel, M. A. *Nature* **1991**, *353*, 737–740.
- (14) Kuang, D.; Brilllet, J.; Chen, P.; Takata, M.; Uchida, S.; Miura, H.; Sumioka, K.; Zakeeruddin, S. M. M. *ACS Nano* **2008**, *2*, 1113–1116.
- (15) Martinson, A. B. F.; Elam, J. W.; Hupp, J. T.; Pellin, M. J. *Nano Lett.* **2007**, *7*, 2183–2187.
- (16) Kang, T. S.; Smith, A. P.; Taylor, B. E.; Durstock, M. F. *Nano Lett.* **2009**, *9*, 601–606.
- (17) Ku, C. H.; Wu, J. *J. Appl. Phys. Lett.* **2007**, *91*, 093117.
- (18) Shankar, K.; Bandara, J.; Paulose, M.; Wietasch, H.; Varghese, O. M.; Mor, G. K.; LaTempa, T. J.; Thelakkat, M.; Grimes, C. A. *Nano Lett.* **2008**, *8*, 1654–1659.
- (19) Leschkies, K. S.; Divakar, R.; Basu, J.; Enache-Pommer, E.; Boercker, J. E.; Carter, C. B.; Kortshagen, U. R.; Norris, D. J.; Aydil, E. S. *Nano Lett.* **2007**, *7*, 1793–1798.
- (20) Sun, W. T.; Yu, Y.; Pan, H. Y.; Gao, X. F.; Chen, Q.; Peng, L. M. *J. Am. Chem. Soc.* **2008**, *130*, 1124–1125.
- (21) Kongkanaed, A.; Tvrđy, K.; Takechi, K.; Kuno, M.; Kamat, P. V. *J. Am. Chem. Soc.* **2008**, *130*, 4007–4015.
- (22) Lee, W.; Kang, S. H.; Kim, J.-Y.; Kolekar, G. B.; Sung, Y.-E.; Han, S. H. *Nanotechnology* **2009**, *20*, 335706.
- (23) Baker, D. R.; Kamat, P. V. *Adv. Funct. Mater.* **2009**, *19*, 805–811.
- (24) Chen, H. M.; Chen, K. C.; Chang, Y.-C.; Tsai, C.-W.; Liu, R. S.; Hu, S. F.; Chang, W.-S.; Chen, K.-H. *Angew. Chem., Int. Ed.* **2010**, *49*, 5966–5969.
- (25) Hodes, G. *J. Phys. Chem. C* **2008**, *112*, 17778–17787.
- (26) Xu, J.; Yang, X.; Wang, H.; Chen, X.; Luan, C.; Xu, Z.; Lu, Z.; Roy, V. A. L.; Zhang, W.; Lee, C.-S. *Nano Lett.* **2011**, *11*, 4138–4143.
- (27) Wang, X.; Zhu, H.; Xu, Y.; Wang, H.; Tao, Y.; Hark, S.; Xiao, X.; Li, Q. *ACS Nano* **2010**, *4*, 3302–3308.
- (28) Tang, Y.; Hu, X.; Chen, M.; Luo, L.; Li, B.; Zhang, L. *Electrochim. Acta* **2009**, *54*, 2742–2747.
- (29) Myung, Y.; Jang, D. M.; Sung, T. K.; Sohn, Y. J.; Jung, B. G.; Cho, Y. J.; Kim, H. S.; Park, J. *ACS Nano* **2010**, *4*, 3789–3800.
- (30) Tak, Y.; Hong, S. J.; Lee, S. J.; Yong, K. *J. Mater. Chem.* **2009**, *19*, 5945–5951.
- (31) Wang, H.; Wang, T.; Wang, X. N.; Liu, R.; Wang, B. Y.; Wang, H. B.; Xu, Y.; Zhang, J.; Duan, J. X. *J. Mater. Chem.* **2012**, *22*, 12532–12537.
- (32) Gan, X.; Li, X.; Gao, X.; Qiu, J.; Zhuge, F. *Nanotechnology* **2011**, *22*, 305601.
- (33) Bang, J. H.; Kamat, P. V. *ACS Nano* **2009**, *3*, 1467–1476.
- (34) Kim, S.-Hm; Fan, D.; Kim, J.-J.; Jung, D. W.; Kang, S. O.; Ko, J. *Electrochem. Commun.* **2009**, *11*, 1337–1339.
- (35) Lee, H.; Bang, J. J.; Park, J.; Kim, S.; Park, S.-M. *Chem. Mater.* **2010**, *22*, 5636–5643.
- (36) Kuo, K.-T.; Liu, D.-M.; Chen, S.-Y.; Lin, C.-C. *J. Mater. Chem.* **2009**, *19*, 6780–6788.
- (37) Salant, A.; Shalom, M.; Hod, I.; Faust, A.; Zaban, A.; Banin, U. *ACS Nano* **2010**, *4*, 5962–968.
- (38) Lee, Y.-L.; Chi, C.-F.; Liau, S.-Y. *Chem. Mater.* **2010**, *22*, 922–927.
- (39) Shen, Q.; Kobayashi, J.; Diguna, L. J.; Toyoda, T. *J. Appl. Phys.* **2008**, *103*, 084304.
- (40) Walle, Van de.; Neugebauer, C. G. *Nature* **2003**, *423*, 626–628.
- (41) Ma, T.; Guo, M.; Zhang, M.; Zhang, Y. J.; Wang, X. D. *Nanotechnology* **2007**, *18*, 035605.
- (42) Duan, J. X.; Wang, H.; Wang, H. B.; Zhang, J.; Wu, S.; Wang, Y. *CrystEngComm* **2012**, *14*, 1330–1336.
- (43) Zeng, H. B.; Duan, G. T.; Li, Y.; Yang, S. K.; Xu, X. X.; Cai, W. P. *Adv. Funct. Mater.* **2010**, *20*, 561–572.
- (44) Tak, Y.; Hong, S. J.; Lee, J. S.; Yong, K. *J. Mater. Chem.* **2009**, *19*, 5945–5951.
- (45) Shokhovets, S.; Ambacher, O.; Gobsch, G. *Phys. Rev. B* **2007**, *76*, 125203.
- (46) Li, L.; Daou, J.; Texier, I.; Chi, T. T. K.; Liem, N. Q.; Reiss, P. *Chem. Mater.* **2009**, *21*, 2422–2429.
- (47) Pons, T.; Pic, E.; Lequeux, N.; Cassette, E.; Benzdetnaya, L.; Guillemain, F.; Marchal, F.; Bubertret, B. *ACS Nano* **2010**, *4*, 2531–2538.
- (48) Park, J.; Kim, S.-W. *J. Mater. Chem.* **2011**, *21*, 3745–3750.
- (49) Wei, S. H.; Zhang, S. B.; Zunger, A. *J. Appl. Phys.* **2000**, *87*, 1304–1311.